Contents lists available at ScienceDirect

Multiple Sclerosis and Related Disorders

journal homepage: www.elsevier.com/locate/msard

Original article

Neurite orientation dispersion and density imaging in myelin oligodendrocyte glycoprotein antibody-associated disease and neuromyelitis optica spectrum disorders

Qianlan Chen [a,b,c], Henri Trang [a,b,c], Patrick Schindler [a,b,c,d,e], Frederike Cosima Oertel [a,b,c,d,e], Tim Hartung [d], Darius Mewes [a,b,c,e,f], Claudia Chien [a,b,c,e,g], Stefan Hetzer [h], Lina Anderhalten [a,b,c,e], Michael Sy [i], Carsten Finke [d], Tanja Schmitz-Hübsch [a,b,c,e], Alexander U. Brandt [a,i,1], Friedemann Paul [a,b,c,d,e,1,*]

[a] Experimental and Clinical Research Center, a cooperation between Max Delbrück Center for Molecular Medicine in the Helmholtz Association and Charité – Universitätsmedizin Berlin, Berlin, Germany
[b] Charité – Universitätsmedizin Berlin, corporate member of Freie Universität Berlin and Humboldt-Universität zu Berlin, Berlin, Germany
[c] Max Delbrück Center for Molecular Medicine in the Helmholtz Association (MDC), Berlin, Germany
[d] Department of Neurology, Charité – Universitätsmedizin Berlin, corporate member of Freie Universität Berlin and Humboldt-Universität zu Berlin, Berlin, Germany
[e] Neuroscience Clinical Research Center, Charité – Universitätsmedizin Berlin, corporate member of Freie Universität Berlin and Humboldt-Universität zu Berlin, Berlin, Germany
[f] Berlin Institute of Health at Charité – Universitätsmedizin Berlin, Biomedical Innovation Academy, Berlin, Germany
[g] Department of Psychiatry and Neurosciences, Charité – Universitätsmedizin Berlin, corporate member of Freie Universität Berlin and Humboldt-Universität zu Berlin, Berlin, Germany
[h] Berlin Center for Advanced Neuroimaging, Charité – Universitätsmedizin Berlin, corporate member of Freie Universität Berlin and Humboldt-Universität zu Berlin, Berlin, Germany
[i] Department of Neurology, University of California Irvine, 208 Sprague Hall, Mail Code 4032, Irvine, CA 92697, USA

ARTICLE INFO

ABSTRACT

Background: Aquaporin-4 antibody positive (AQP4+) neuromyelitis optica spectrum disorders (NMOSD) and myelin oligodendrocyte glycoprotein antibody-associated disease (MOGAD) are two distinct antibody-mediated neuroinflammatory diseases. Diffusion Tensor Imaging (DTI) and Neurite Orientation Dispersion and Density Imaging (NODDI) are advanced diffusion-weighted MRI models providing quantitative metrics sensitive to cerebral microstructural changes. This study aims to differentiate brain tissue damage in NMOSD and MOGAD from controls and investigate its association with clinical disability, using NODDI and DTI-derived measures, including fractional anisotropy (FA), mean diffusivity (MD), axial diffusivity (AD) and radial diffusivity.
Methods: This study included 31 AQP4+ NMOSD, 21 MOGAD patients and 45 healthy controls. Clinical information included disease duration, Expanded Disability Status Scale (EDSS), Timed 25 Foot Walk test (T25FW), Nine-Hole Peg Test (9HPT), Symbol Digit Modalities Test (SDMT) and monocular 100 % high contrast visual acuity (HCVA). All participants underwent MRI scanning with multi-shell diffusion-weighted imaging, T2w fluid-attenuated inversion recovery and T1w magnetization prepared–rapid acquisition gradient echo sequences to obtain manually segmented T2-hyperintense white matter lesions (WML) and normal-appearing brain tissue (NABT) masks, including white matter (NAWM), cortical and deep gray matter (NACGM, NADGM). DTI and NODDI metrics were compared between groups using region-of-interest (ROI) analysis and tract-based spatial statistics. Tissue-weighted means were obtained for the NODDI metrics (weighted neurite density index, wNDI; weighted orientation dispersion index, wODI). Group differences in ROI analyses were assessed using age and sex adjusted linear regression models, followed by post-hoc comparisons with estimated marginal means. Stepwise multivariable linear regression models were used to evaluate the association between MRI biomarkers and clinical outcomes.

Results: NMOSD patients had higher T2 lesion volume (1120.5 mm^3 vs. 374.6 mm^3, $p<$.001) and number (median 22 vs. 6, $p<$.001) than MOGAD patients. Both NMOSD and MOGAD lesions displayed lower wNDI and higher isotropic volume fraction (ISOVF) compared to microvascular lesions in controls ($p<$.05). In NACGM, NMOSD patients showed higher wODI but lower ISOVF compared to HC ($p=$.029). MOGAD patients had lower wNDI in NACGM compared to NMOSD ($p=$.012). Tract-based spatial statistics revealed damage to specific white matter abnormalities in NMOSD, with higher AD, ODI and ISOVF compared to controls, particularly in the corpus callosum and corticospinal tract. Clinical associations in NMOSD included higher EDSS with higher NAWM ISOVF (R^2=0.46, $p=$.006), higher 9HPT with lower intralesional FA and higher NAWM MD (R^2=0.54, $p=$.022), lower SDMT with lower intralesional FA and higher NACGM ISOVF (R^2=0.54, $p=$.013), worse visual acuity with higher NAWM wODI. In MOGAD, higher EDSS was associated with lower NAWM FA (R^2=0.29, $p=$.022), slower T25FW with higher NADGM ISOVF (R^2=0.48, $p<$.001), lower SDMT with higher NAWM ISOVF (R^2=0.62, $p=$.005) and worse visual acuity with higher NADGM MD.

Conclusion: NODDI and DTI measures are sensitive to pathological alterations in myelin and axon integrity, as water diffusion is less restricted in demyelinated tissue. Compared to MOGAD, patients with NMOSD tend to exhibit more extensive chronic white matter damage, demyelination or axonal injury. NODDI demonstrates greater sensitivity and specificity to alterations in NACGM compared to DTI. Given their association with clinical disability, NODDI metrics appear to be valuable neuroimaging biomarkers for assessing microstructural damage in clinical research.

1. Introduction

Myelin oligodendrocyte glycoprotein antibody-associated disease (MOGAD) and aquaporin-4 antibody positive (AQP4+) neuromyelitis optica spectrum disorder (NMOSD) are two distinct autoimmune inflammatory diseases of the central nervous system, which share overlapping clinical phenotypes including relapsing optic neuritis and myelitis. While AQP4+ NMOSD is an antibody-mediated astrocytopathy (Jarius et al., 2020; Papadopoulos and Verkman, 2012), MOGAD is regarded as an antibody-mediated oligodendrocytopathy (Banwell et al., 2023; Jarius et al., 2018). Although both diseases are primarily diagnosed based on antibody testing and clinical phenotype, magnetic resonance imaging (MRI) of brain and spinal cord demonstrate diagnostically relevant findings, e.g., in white matter lesion location and appearance (Banwell et al., 2023; Wingerchuk DM, 2015).

Diffusion tensor imaging (DTI) measures the diffusion of water molecules along the direction of axonal bundles and can detect microstructural brain abnormalities which conventional MRI is unable to display. Derived parameters from DTI include fractional anisotropy (FA), mean diffusivity (MD), axial diffusivity (AD) and radial diffusivity (RD) (Alexander et al., 2007). Lower FA is associated with axonal loss or axonal damage. However, DTI has its limitations. It assumes that water diffusion is primarily restricted to a single fiber direction within a single voxel, which does not hold true in regions with complex fiber crossings and multiple fiber orientations. Moreover, since diffusion is relatively isotropic in gray matter, DTI is not sensitive to explore abnormalities of gray matter (Wheeler-Kingshott and Cercignani, 2009). Neurite orientation dispersion and density imaging (NODDI) is an advanced multi-compartment diffusion MRI model that probes the microstructure of axons and dendrites by simulating three subdivisions of the brain tissue, and provides three metrics: 1) neurite density index (NDI) refers to the "neurite density" or "intra-cellular restricted diffusion" within the intra-cellular compartment. NDI reduction may indicate axonal loss or damage; 2) orientation dispersion index (ODI) measures the variability in neurite dispersion, an increased ODI suggests disorganized neurite structures and 3) isotropic volume fraction (ISOVF) represents the fraction of the extracellular free water, that increases with loss of tissue integrity or edema linked to inflammation (Zhang et al., 2012). NODDI is able to overcome the limitation of non-specific changes in DTI parameters, such as disentangling the different microstructural contributions on fractional anisotropy. As such, NODDI has been applied in several neurological disorders including NMOSD, multiple sclerosis, stroke and Parkinson's disease (Andica et al., 2022; Bagdasarian et al., 2021; Kato et al., 2022; Mitchell et al., 2022). Notably, NODDI has demonstrated improved sensitivity in detecting microstructural changes in multiple sclerosis, showing widespread NDI reduction (pronounced

axonal damage) in both focal lesions and normal-appearing white matter (Rahmanzadeh et al., 2021). The microstructural alterations derived from NODDI in MOGAD remain incompletely elucidated (Sun et al., 2023).

Against this background, the aim of this cross-sectional cohort study was to 1) investigate microstructural tissue differences between AQP4+ NMOSD and MOGAD patients compared to healthy controls using NODDI and DTI; and 2) explore the correlation between NODDI-derived and DTI-derived biomarkers with clinical disability.

2. Materials and methods

2.1. Participants

From October 2019 to February 2023, a total of 52 patients (31 AQP4+ NMOSD, 21 MOGAD) and 45 healthy controls were included in this study (Table 1). Patient data for this retrospective cross-sectional study were derived from two monocentric observational studies at the Neuroscience Clinical Research Center (NCRC), Charité – Universitätsmedizin Berlin, Germany. All patients were enrolled in the NMO cohort study, which was then superseded by the ongoing BERLimmun registry study (Sperber et al., 2022). Patients were recruited from inpatient and outpatient neuroimmunology services at Charité – Universitätsmedizin Berlin. Inclusion criteria were (1) age over 18 years and (2) the diagnosis of AQP4+ NMOSD according to the international panel criteria for NMOSD diagnosis (Wingerchuk DM, 2015) or the diagnosis of MOGAD based on suggested diagnostic criteria of MOG encephalomyelitis (Jarius et al., 2018). All MOGAD patients fulfilled the meanwhile published international consensus diagnostic criteria for MOGAD (Banwell et al., 2023). Exclusion criteria were (1) MRI contraindications (i.e., claustrophobia), (2) insufficient MRI image quality, and (3) a history of other neurologic/psychiatric disorders. Cell-based assay (CBA) testing methods were applied for AQP4-immunoglobulin G (IgG) (fixed CBA, Euroimmun, Luebeck, Germany) and MOG-IgG (live CBA) serological antibody detection (Jarius et al., 2018). Data from forty-five age-matched controls without neurological or psychiatric disorders were derived from two ongoing registry studies (BERLimmun and CAMINO) (Heine et al., 2023; Sperber et al., 2022).

2.2. Clinical examination

Clinical parameters collected for patients included age, sex, time from symptom onset to the visit date (herein referred to as "disease duration"), number of attacks, Expanded Disability Status Scale (EDSS) score, Timed 25 Foot Walk (T25FW) test, Nine-Hole Peg Test (9HPT) in both dominant-hand and non-dominant hand, symbol digit modalities

Table 1
Demographic and clinical characteristics of the subjects.

	MOGAD	AQP4-IgG+ NMOSD	HC	Statistics	P value
Number of subjects [n] (total = 97)	21	31	45		
Number of subjects with cerebral lesions [n] (percentage)	19 (90.5 %)	29 (93.5 %)	32 (71.1 %)	$X^2 = 7.580$	**0.023**
Age [years], mean (SD)	41 (17)	43 (19)	44 (15)	$F = 0.162$	0.851
Female/male [n] (% female)	14F/7M (67 %)	29F/2M (94 %)	36F/9M (80 %)	$X^2 = 6.101$	0.047
EDSS, median (IQR)	2.0 (1.5, 3.5)	3.5 (2, 4)	NA	$W = 377$	0.195
Disease duration (since symptom onset) [years], median (IQR)	2.8 (0.6, 8.8)	9.4 (7.1, 11.3)	NA	$W = 481$	**0.003**
Interval from last attack to MRI examination [months], median (IQR)	18.2 (6.6, 33.3)	70.6 (32.0, 102.6)	NA	$W = 486$	**0.002**
Number of relapses, median (IQR)	2 (1, 6)	3 (2, 4)	NA	$W = 371.5$	0.388
Clinical phenotype					
ON only, [n] (%)	13 (62 %)	8 (26 %)	NA	$X^2 = 5.360$	**0.021**
Myelitis only, [n] (%)	3 (14 %)	14 (45 %)	NA	$X^2 = 4.111$	**0.043**
ON + Myelitis, [n] (%)	4 (19 %)	7 (23 %)	NA		
Area postrema syndrome, [n] (%)	0	2 (6 %)	NA	$X^2 = 0.204$	0.651
Cerebral syndrome*, [n] (%)	1 (5 %)	0	NA	$X^2 = 0.039$	0.843
ADEM, [n] (%)	0	0	NA		
Subjects with symptomatic brain lesions, [n] (%)	1 (5 %)	0	NA	$X^2 = 0.039$	0.843
T2 Lesion volume [mm³], median (IQR)	374.6 (54.0, 1096.9)	1120.5 (502.9, 2397.9)	104.6 (36.3, 496.1)	$H = 16.557$	< **0.001**
T2 Lesion number, median (IQR)	6 (2, 13)	22 (10, 45)	5 (2, 10)	$H = 17.23$	< **0.001**
Brain lesion location					
Cortical/juxtacortical, [n] (%)	6 (29 %)	1 (3 %)	NA	$X^2 = 4.899$	**0.027**
Deep gray matter, [n] (%)	0	4 (13 %)	NA	$X^2 = 1.400$	0.237
T25FW speed [m/s], mean (SD)	1.8 (0.3)	1.4 (0.4)	NA	$t = -4.014$	< **0.001**
9HPTdom speed [peg/s], mean (SD)	0.44 (0.08)	0.45 (0.08)	NA	$t = 0.179$	0.859
9HPTndom speed [peg/s], mean (SD)	0.41 (0.07)	0.42 (0.09)	NA	$t = 0.361$	0.719
SDMT, mean (SD)	54 (14)	52 (15)	NA	$t = -0.514$	0.610
HCVA worse eye [logMAR], median (IQR)	−0.1 (−0.2, 0.2)	0.1 (−0.1, 0.4)	NA	$W = 368.5$	0.108
HCVA better eye [logMAR], median (IQR)	−0.2 (−0.2, −0.1)	−0.1 (−0.2, 0)	NA	$W = 379$	0.060

Abbreviations:
HC, healthy control; MOGAD, Myelin Oligodendrocyte Glycoprotein Antibody-associated Disease AQP4-IgG+ NMOSD, aquaporin-4 antibody seropositive Neuromyelitis Optica Spectrum Disorder; EDSS, Expanded Disability Status Scale; ON, Optic Neuritis; ADEM, Acute Disseminated Encephalomyelitis; T25FW, Timed 25 Foot Walk; 9HPTdom, dominant hand of nine-hole peg test; 9HPTndom, non-dominant hand of nine-hole peg test; SDMT, Symbol Digit Modalities Test; HCVA, High Contrast Visual Acuity; logMAR, logarithm of the Minimum Angle of Resolution; SD, standard deviation, IQR, interquartile range; H represents the statistic of Kruskal-Wallis H test; X^2 represents the statistic of Chi-square test; F represents the statistic in one way Analysis of Variance; t represents the statistic in unpaired Student's t-test; W represents the statistic in Wilcoxon rank-sum test; NA: not applicable. Bold p value indicate statistical significance.
*Cerebral syndrome represents headache syndrome with symptomatic epilepsy.

test (SDMT) and monocular 100 % high contrast visual acuity (HCVA) measurement using a high-contrast Early Treatment Diabetic Retinopathy Study (ETDRS) chart (at 4 m). T25FW and 9HPT tests were performed twice, measurements averaged, and then converted from performance time to speed for further analysis (Grobelny et al., 2017; Lamers et al., 2015), with higher speed meaning better results. Visual acuity was measured as decimal acuity and then converted to the logarithm of the Minimum Angle of Resolution (logMAR) with higher logMAR values meaning worse vision. All clinical examinations were performed by trained study personnel under procedural supervision of board-certified neurologists.

2.3. Ethics approval

This study was approved by the institutional ethics committee of Charité – Universitätsmedizin Berlin, Germany as part of the underlying observational studies (approval numbers of NMO cohort study, BER-Limmun and CAMINO, EA1/041/14, EA1/362/20 and EA2/007/21 respectively) (Heine et al., 2023; Sperber et al., 2022). The study's conduct was in accordance with the 1964 Declaration of Helsinki in its applicable version. All participants provided written informed consent prior to participation in the study.

2.4. Magnetic resonance imaging

MRI data were acquired at the Berlin Center for Advanced Neuro-imaging (BCAN) using a 3.0T PRISMA MR system (Siemens Healthineers, Erlangen, Germany) and a 64-channel head-neck coil. From the imaging protocol, the following sequences were included in this study: (1) 3D T1-weighted magnetization prepared-rapid acquisition gradient echo (MPRAGE): 0.8mm resolution isotropic, repetition time (TR)= 2,500ms, echo time (TE)=2.22ms, field of view (FOV)=256×256mm, inversion time (TI)=1,000ms, matrix 320×320, flip angle=8°; (2) 3D T2-weighted fluid-attenuated inversion recovery (FLAIR): 0.8mm resolution, TR=6,000ms, TE=387ms, FOV=256×256mm, TI=2,100ms, matrix 320×320, flip angle=120°; (3) whole brain multi-shell diffusion-weighted imaging: 1.5mm isotropic resolution, TR=3,230ms, TE=89.2ms, flip angle=120°, with 99 diffusion directions (b-value=5s/mm²[7], 1,500s/mm²[46], and 3000 s/mm²[46]) (Michael P et al., 2018).

Diffusion MRI preprocessing included denoising with MRtrix3 (Tournier et al., 2019), eddy current and distortion correction, and brain extraction using FMRIB Software Library (FSL) (version v6.0, FMRIB, Oxford, UK). For the reconstruction of DTI-derived parametric maps, the preprocessed diffusion MRI with b-values of 5 and 1500 s/mm² were fitted into a DTI model (dtifit in FSL) to produce fractional anisotropy (FA), mean diffusivity (MD), axial diffusivity (AD) and radial diffusivity (RD). For NODDI fitting, all preprocessed diffusion MRI volumes were utilized to compute NDI, ODI, and ISOVF parametric maps with the accelerated microstructure imaging via convex optimization (AMICO) tool (Daducci et al., 2015) (Fig. 1).

To perform voxelwise comparison in tract-based spatial statistics (TBSS), FA maps for all participants were aligned with the Montreal Neurological Institute 152 standard space. This involved averaging and skeletonization of the FA images after alignment, which highlighted the central regions of the WM tracts that were consistent among all individuals. The average FA skeleton was then filtered by setting a threshold to 0.2, excluding outer tracts and gray matter (Smith et al.,
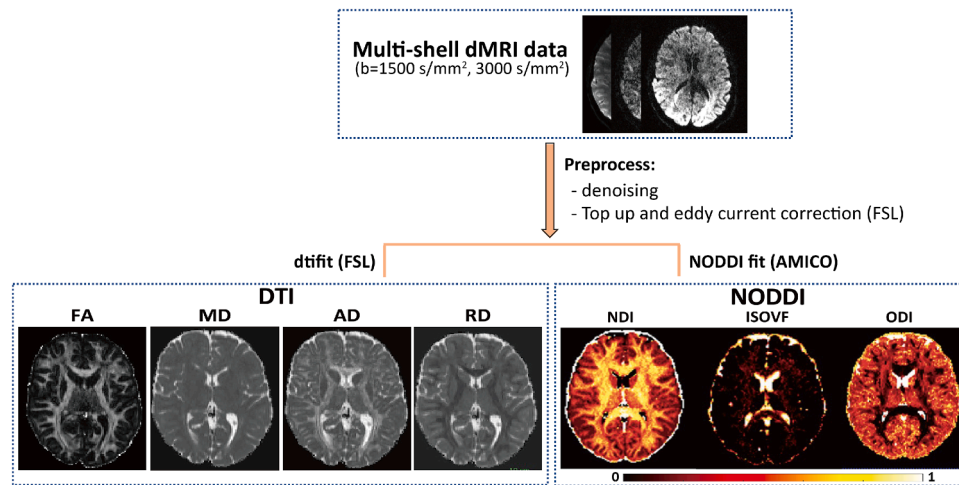
Fig. 1. Analysis pipeline.
Example of DTI-derived and NODDI-derived parametric maps. DTI: diffusion tensor imaging; FA: fractional anisotropy; MD: mean diffusivity; AD: axial diffusivity; RD: radial diffusivity; NODDI: neurite orientation dispersion and density imaging; NDI: neurite density index; ISOVF: isotropic volume fraction; ODI: orientation dispersion index; FSL: FMRIB Software Library; AMICO: accelerated microstructure imaging via convex optimization.

2006). Following this, the FA map of each subject was aligned and projected onto this skeleton. This projection involved assigning the highest FA value along the vertical line for each voxel. The other DTI-derived maps (AD, MD, and RD), NODDI-derived maps (ODI, ISOVF, and NDI) were then projected onto the average FA skeleton as well, utilizing the deformation field from the alignment of each subject's data to the standard space.

Involvement of brain lesions on conventional MRI was recorded in all patient groups. White matter lesions (WML) were defined as T2-hyperintense from FLAIR and binarized WML masks were created manually by two experienced raters (>15 years of experience) using ITK-SNAP (version 3.8.0; http://www.itksnap.org/) (Yushkevich et al., 2016). Lesion-filled MPRAGE images (ANTs, version 2.4.3) were used to obtain tissue segmentation of normal-appearing cortical gray matter (NACGM), normal-appearing deep gray matter (NADGM) and white matter (WM) using FastSurfer (Henschel et al., 2020). The normal-appearing WM (NAWM) mask was obtained after lesion subtraction from the whole brain WM mask. NADGM masks contained bilateral thalamus, pallidum, caudate, putamen, hippocampus, amygdala and nucleus accumbens. The segmented tissue masks and binarized lesion masks were co-registered with the first b0 diffusion volume before extracting region-specific DTI and NODDI values using fslstats in FSL. We applied the tissue-weighted mean method proposed by Parker et al. (Parker et al., 2021) on NODDI metrics to reduce partial volume effects mainly caused by cerebrospinal fluid contamination. The subsequent analysis of group differences used the calculated tissue-weighted means of NDI (wNDI) and ODI (wODI).

2.5. Statistical analysis

All statistical analyses were performed in R (version 4.1.2, http://www.r-project.org/). For demographic and disease-related cohort data, categorical data were compared with chi-square test, and continuous variables were compared with Mann-Whitney U test, unpaired Student's *t*-test or Kruskal-Wallis H test dependent on their scale.

Group differences in the region-of-interest (ROI) analyses in each tissue class were assessed using linear regression models with age and sex as covariates followed by post-hoc comparisons using estimated marginal means ("emmeans" R package) to account for the influence of covariates. The effect size of group differences in different tissue classes was evaluated using Cohen's d. The magnitude of the Cohen's d was defined as small (0.2–0.5), medium (0.5–0.8) and large ($d \geq 0.8$) effect size (Lakens, 2013). $P<.05$ was regarded as statistically significant.

Correlation between disease duration and MRI variables were examined using Spearman rank-order coefficient (rho).

White matter lesion masks were co-registered to the B0 volume and then registered non-linearly to the TBSS skeleton space. The lesion voxels were excluded from the subsequent voxelwise comparisons using FSL "setup_masks". The FSL nonparametric permutation analysis tool *randomise* was used to calculate voxelwise statistics among the three groups. The designed matrix included age and sex as covariates. The permutation tests were performed using *randomise* with 5000 permutations, and the significance threshold was set at $P<.05$ with Family-wise Error (FWE), corrected for multiple comparisons using threshold-free cluster enhancement (TFCE). The JHU-ICBM-DTI-81 WM atlas was used to identify the location of WM tracts that contained clusters with significant differences (Mori et al., 2008).

To analyze associations with clinical disability, we first performed univariate linear regression models to select statistically significant independent metrics after removing AD and RD to reduce collinearity. We retained FA and MD, the most informative and widely used DTI metrics in neurological disorders (Haddad et al., 2022), along with all NODDI-derived metrics to explore their clinical relevance. Using this approach, some independent variables in the multivariate regression model were collinear (cutoff: Variance Inflation Factor (VIF) >5). Subsequently, we applied forward stepwise ordinary least square (OLS) linear regression models ("olsrr" R package) for each disease group, with clinical outcome as dependent variable, and age and MRI markers as independent variables. Optimal variable selection was based on $P<.05$.

3. Results

3.1. Voxel-wise DTI and NODDI

3.1.1. White matter lesions

Table 2 summarizes DTI/NODDI-derived parameters and comparisons among groups. WML displayed similar characteristics in MOGAD and NMOSD in contrast to HC in DTI and NODDI findings. WML in MOGAD patients had higher MD, AD, and RD compared to the cerebral small vascular-related WML in HC, with similar findings observed in patients with NMOSD. For the NODDI metrics, WML in MOGAD patients had significantly lower wNDI but higher ISOVF compared to HC (Fig. 2A). WML in patients with NMOSD also showed lower wNDI and higher ISOVF against HC (Fig. 2A). WML among patient groups and healthy controls in wODI and FA did not differ significantly.

Table 2
Linear model results of DTI and NODDI parameters.

Groups	MOGAD	NMOSD	HC	MOGAD - HC		NMOSD - HC		NMOSD - MOGAD	
	values, mean (SD)			Cohen's d (95 %CI)	P[a]	Cohen's d (95 %CI)	P[a]	Cohen's d (95 %CI)	P[a]
WML									
wNDI	0.381 (0.136)	0.43 (0.083)	0.476 (0.07)	−1.48 (−2.17, −0.78)	**<0.001**	−0.90 (−1.47, −0.32)	**0.002**	0.68 (−0.02, 1.38)	0.052
wODI	0.241 (0.091)	0.213 (0.048)	0.237 (0.061)	−0.22 (−0.84, 0.40)	0.476	−0.35 (−0.90, 0.20)	0.204	−0.33 (−1.01, 0.36)	0.342
ISOVF	0.204 (0.071)	0.212 (0.081)	0.149 (0.057)	0.83 (0.18, 1.48)	**0.011**	0.87 (0.30, 1.44)	**0.002**	0.03 (−0.64, 0.70)	0.926
FA	0.308 (0.108)	0.349 (0.052)	0.36 (0.074)	−0.51 (−1.14, 0.11)	0.100	−0.42 (−0.97, 0.13)	0.128	0.64 (−0.06, 1.34)	0.066
MD (10^{-3}mm^2/s)	0.963 (0.147)	0.932 (0.095)	0.806 (0.073)	1.60 (0.89, 2.31)	**<0.001**	1.68 (1.04, 2.31)	**<0.001**	−0.39 (−1.10, 0.31)	0.265
RD (10^{-3}mm^2/s)	0.806 (0.175)	0.756 (0.1)	0.645 (0.085)	1.30 (0.61, 1.98)	**<0.001**	1.44 (0.83, 2.05)	**<0.001**	−0.34 (−1.03, 0.35)	0.323
AD (10^{-3}mm^2/s)	1.278 (0.151)	1.286 (0.11)	1.127 (0.113)	1.19 (0.51, 1.86)	**<0.001**	1.65 (1.02, 2.28)	**<0.001**	0.15 (−0.55, 0.86)	0.662
NAWM									
wNDI	0.522 (0.035)	0.516 (0.036)	0.524 (0.025)	−0.13 (−0.69, 0.42)	0.630	−0.12 (−0.60, 0.35)	0.604	0.21 (−0.41, 0.82)	0.500
wODI	0.284 (0.016)	0.286 (0.013)	0.28 (0.013)	0.19 (−0.36, 0.74)	0.495	0.48 (−0.01, 0.98)	0.051	0.43 (−0.2, 1.06)	0.170
ISOVF	0.159 (0.02)	0.159 (0.024)	0.159 (0.022)	0.20 (−0.35, 0.74)	0.472	0.28 (−0.20, 0.76)	0.246	−0.18 (−0.81, 0.46)	0.578
FA	0.374 (0.024)	0.369 (0.022)	0.376 (0.02)	−0.39 (−0.94, 0.16)	0.156	−0.29 (−0.78, 0.19)	0.230	0 (−0.61, 0.61)	1.000
MD (10^{-3}mm^2/s)	0.706 (0.027)	0.709 (0.032)	0.705 (0.024)	0.19 (−0.35, 0.74)	0.476	0.25 (−0.23, 0.73)	0.308	−0.28 (−0.91, 0.35)	0.373
RD (10^{-3}mm^2/s)	0.557 (0.034)	0.561 (0.036)	0.555 (0.03)	0.23 (−0.31, 0.77)	0.400	0.33 (−0.15, 0.81)	0.178	−0.22 (−0.85, 0.41)	0.481
AD (10^{-3}mm^2/s)	1.005 (0.02)	1.005 (0.027)	1.006 (0.017)	0.17 (−0.38, 0.71)	0.543	−0.17 (−0.66, 0.32)	0.500	−0.3 (−0.93, 0.33)	0.343
NADGM									
wNDI	0.463 (0.046)	0.451 (0.04)	0.455 (0.034)	0.20 (−0.34, 0.74)	0.456	0.08 (−0.41, 0.57)	0.751	0.02 (−0.61, 0.65)	0.942
wODI	0.381 (0.016)	0.38 (0.014)	0.379 (0.018)	0.07 (−0.47, 0.61)	0.788	0.15 (−0.32, 0.63)	0.521	0.21 (−0.41, 0.82)	0.502
ISOVF	0.191 (0.028)	0.193 (0.021)	0.202 (0.035)	−0.28 (−0.83, 0.26)	0.305	−0.32 (−0.79, 0.16)	0.190	0.08 (−0.56, 0.72)	0.795
FA	0.274 (0.012)	0.269 (0.01)	0.273 (0.015)	0.07 (−0.47, 0.60)	0.809	−0.12 (−0.60, 0.36)	0.629	−0.35 (−0.98, 0.29)	0.276
MD (10^{-3}mm^2/s)	0.714 (0.021)	0.721 (0.025)	0.724 (0.025)	−0.36 (−0.91, 0.18)	0.185	−0.13 (−0.61, 0.34)	0.585	0.05 (−0.57, 0.66)	0.882
RD (10^{-3}mm^2/s)	0.608 (0.021)	0.616 (0.024)	0.617 (0.024)	−0.34 (−0.88, 0.21)	0.222	−0.07 (−0.54, 0.41)	0.773	0.07 (−0.54, 0.68)	0.818
AD (10^{-3}mm^2/s)	0.925 (0.023)	0.93 (0.029)	0.937 (0.03)	−0.33 (−0.88, 0.21)	0.223	−0.22 (−0.7, 0.25)	0.354	0.05 (−0.56, 0.67)	0.868
NACGM									
wNDI	0.360 (0.027)	0.365 (0.022)	0.360 (0.017)	−0.26 (−0.81, 0.29)	0.347	0.16 (−0.32, 0.64)	0.510	0.81 (0.16, 1.46)	**0.012**
wODI	0.433 (0.014)	0.435 (0.013)	0.429 (0.012)	0.31 (−0.23, 0.85)	0.254	0.54 (0.05, 1.02)	**0.029**	0.24 (−0.38, 0.87)	0.434
ISOVF	0.452 (0.038)	0.454 (0.032)	0.474 (0.042)	−0.38 (−0.93, 0.17)	0.164	−0.67 (−1.17, −0.18)	**0.007**	−0.41 (−1.04, 0.22)	0.193
FA	0.177 (0.012)	0.176 (0.009)	0.177 (0.009)	−0.34 (−0.89, 0.21)	0.223	−0.05 (−0.53, 0.43)	0.829	0.64 (0, 1.28)	0.050
MD (10^{-3}mm^2/s)	0.872 (0.053)	0.879 (0.047)	0.881 (0.044)	−0.28 (−0.84, 0.27)	0.310	−0.08 (−0.56, 0.41)	0.750	0.24 (−0.39, 0.87)	0.442
RD (10^{-3}mm^2/s)	0.803 (0.052)	0.81 (0.045)	0.812 (0.044)	−0.29 (−0.85, 0.27)	0.299	−0.07 (−0.55, 0.41)	0.772	0.25 (−0.37, 0.88)	0.417
AD (10^{-3}mm^2/s)	1.009 (0.054)	1.016 (0.051)	1.019 (0.045)	−0.27 (−0.82, 0.29)	0.334	−0.08 (−0.57, 0.41)	0.734	0.24 (−0.39, 0.86)	0.453

[a] A linear regression model was used adjusting for age and sex.

Abbreviations: MOGAD: myelin oligodendrocyte glycoprotein antibody-associated disease; NMOSD: Neuromyelitis Optica Spectrum disorder; HC: healthy control; WML: white matter lesion; NAWM: normal appearing white matter; NADGM: normal appearing deep gray matter; NACGM: normal appearing cortical gray matter; wNDI: tissue-weighted mean of neurite density index; wODI: tissue-weighted mean of orientation dispersion index; ISOVF: isotropic volume fraction; FA: fractional anisotropy; MD: mean diffusivity; AD: axial diffusivity; RD: radial diffusivity; 95 %CI: confidence interval.

3.1.2. Normal-appearing white matter

In the ROI analysis, there was no significant difference between patients and HC with respect to NAWM in either DTI-derived or NODDI-derived parameters.

3.1.3. Normal-appearing gray matter

Patients with NMOSD had higher wODI in NACGM in contrast to HC, while NACGM ISOVF showed a decreasing trend in NMOSD (Fig. 2D). The only significant difference between MOGAD and NMOSD was lower wNDI in NACGM of patients with MOGAD compared to NMOSD
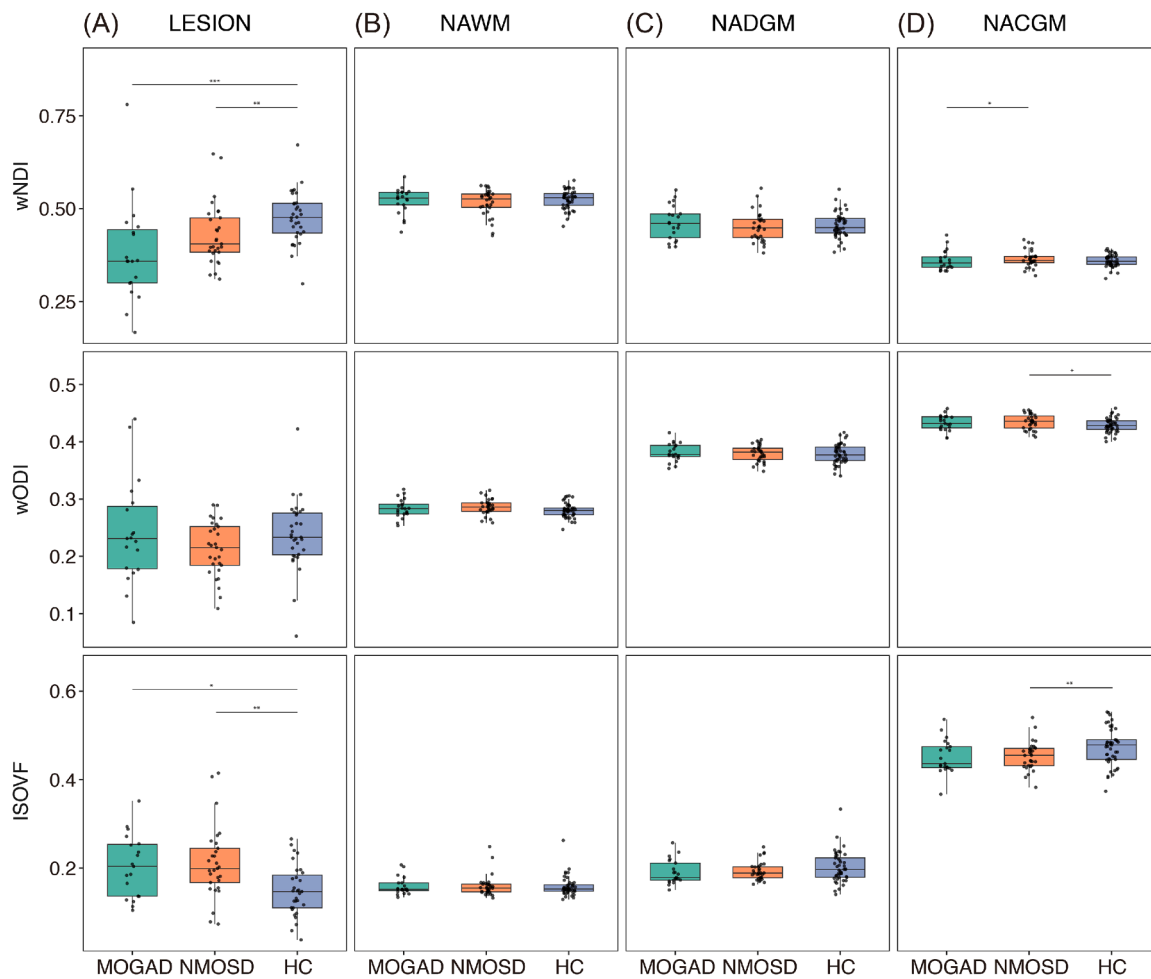
Fig. 2. Groupwise comparison of NODDI in different regions of interest.
(A) LESION; (B) NAWM; (C) NADGM; (D) NACGM. The 25th, median and 75th percentiles are marked with boxplots, and the outliers are marked by points. Asterisks indicate significant differences among the groups: *, $p<.05$; **, $p<.01$; ***, $p<.001$. NAWM, normal-appearing white matter; NADGM, normal-appearing deep gray matter; NACGM, normal-appearing cortical gray matter; wNDI, weighted neurite density index; wODI, weighted orientation dispersion index; ISOVF, isotropic volume fraction; MOGAD, myelin oligodendrocyte glycoprotein antibody-associated disease; NMOSD, neuromyelitis optica spectrum disorder; HC, healthy control.

patients, however, without any significant difference from controls (Fig. 2D). In NACGM, we found no significant differences within standard DTI-derived metrics. In NADGM, no significant difference between patients and HC was found in either DTI or NODDI-derived parameters.

3.2. Tract-based spatial statistics

Patients with NMOSD presented white matter abnormalities in several regions compared to HC (Fig. 3). NMOSD patients had significantly higher AD in the corpus callosum body compared to HC ($p=.019$, TFCE-corrected). Tracts with higher ODI were located in bilateral cerebral peduncles and the bilateral posterior limb of the internal capsule ($p=.001$, TFCE-corrected). ISOVF was significantly higher in the corpus callosum body, right superior corona radiata, right superior longitudinal fasciculus and right corticospinal tract of the NMOSD group ($p=.018$, TFCE-corrected). Other tract-based parameter analyses did not reveal any significant difference in NMOSD and a similar analysis in MOGAD patients showed no difference compared to HC in any DTI- or NODDI-derived parameters (data not shown).

Moreover, we have conducted a ROI analysis based on white matter tracts involved in the sensorimotor pathways among NMOSD patients with/without myelitis. The sensitivity analysis showed that lower FA and lower AD in the cerebral peduncles in NMOSD patients without myelitis and higher ISOVF in right superior longitudinal fasciculus

compared to HC. NMOSD patients with myelitis showed more extensive alterations compared to HC, including higher MD and higher AD in body of corpus callosum and right superior corona radiata, higher RD but lower NDI in right corticospinal tract, and higher ISOVF in the body of corpus callosum.

3.3. Association between DTI and NODDI parameters and clinical disability

Lastly, we investigated associations of DTI/NODDI parameters with clinical disability separately for patients diagnosed with NMOSD and MOGAD (Fig. 4, **Supplementary Table 1**). Our multicollinearity assessment revealed that NAWM-MD and NAWM-NDI exhibited intercorrelations (VIF>5) among diffusion metrics. Associations of clinical outcomes were weaker with diffusion MRI biomarkers in MOGAD patients than in NMOSD. Notably, many clinical outcomes were associated with age, which we therefore included as an independent variable in the stepwise regression model.

3.3.1. Normal-appearing white matter

In patients with NMOSD, we found that worse EDSS was associated with higher ISOVF in NAWM. Reduced 9HPT speed of the dominant hand was associated with higher NAWM MD. Slower 9HPT speed of the non-dominant hand was associated with lower NAWM FA. Worse visual
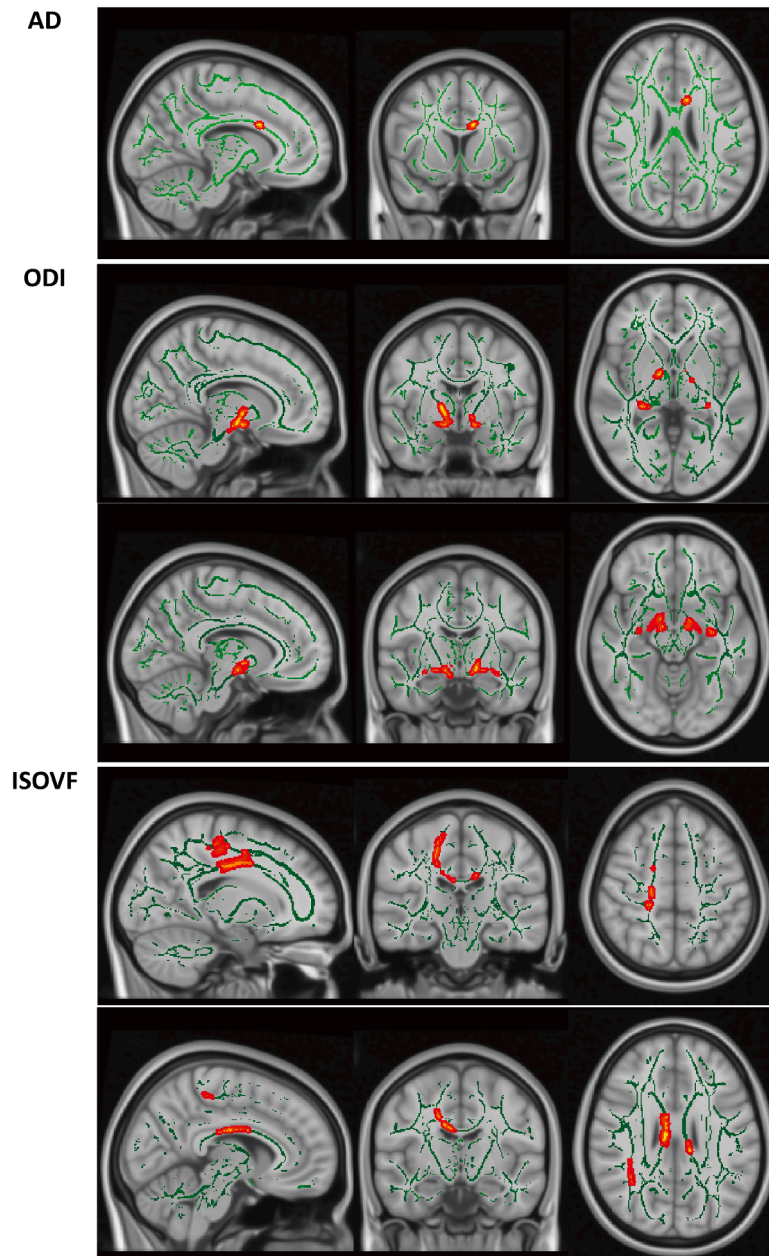
NMOSD - HC

Fig. 3. Group differences between NMOSD and HC demonstrated by TBSS.
Results of voxelwise comparisons between NMOSD and HC on AD, ODI, and ISOVF respectively. Green regions represent the mean FA skeleton overlaid on the MNI152 template. Red-yellow regions represent the brain regions with significantly increased AD, ODI, and ISOVF in NMOSD patients. NMOSD, neuromyelitis optica spectrum disorder; HC, healthy control; AD, axial diffusivity; ODI, orientation dispersion index; ISOVF, isotropic volume fraction.

acuity (unilateral and mean scores) was associated with higher NAWM wODI. Disease duration showed significant positive correlations with both ISOVF and wODI of normal-appearing white matter (rho = 0.52, p=.002 and rho = 0.39, p=.029, respectively).

In patients with MOGAD, higher EDSS was associated with lower NAWM FA. Worse SDMT scores were strongly associated with higher NAWM ISOVF.

3.3.2. White matter lesions

In patients with NMOSD, reduced 9HPT speed of the dominant hand and worse SDMT scores were both associated with lower lesional FA.

3.3.3. Normal-appearing gray matter

In NMOSD, worse T25FW disability was strongly associated with higher ISOVF values in NADGM. Worse SDMT scores were associated with higher NACGM ISOVF.

In MOGAD patients, Slower T25FW speed was associated with higher NADGM ISOVF. We did not find any association between 9HPT speed of the dominant hand and the investigated NODDI/DTI metrics. Reduced visual acuity was associated with higher NADGM MD. Disease duration exhibited significant correlations with cortical gray matter damage. Positive correlations were observed with RD and ISOVF (rho= 0.45, p=.037 and rho = 0.52, p=.017, respectively), Conversely, a negative correlation was found with FA in NACGM (rho = −0.43, p=.049).
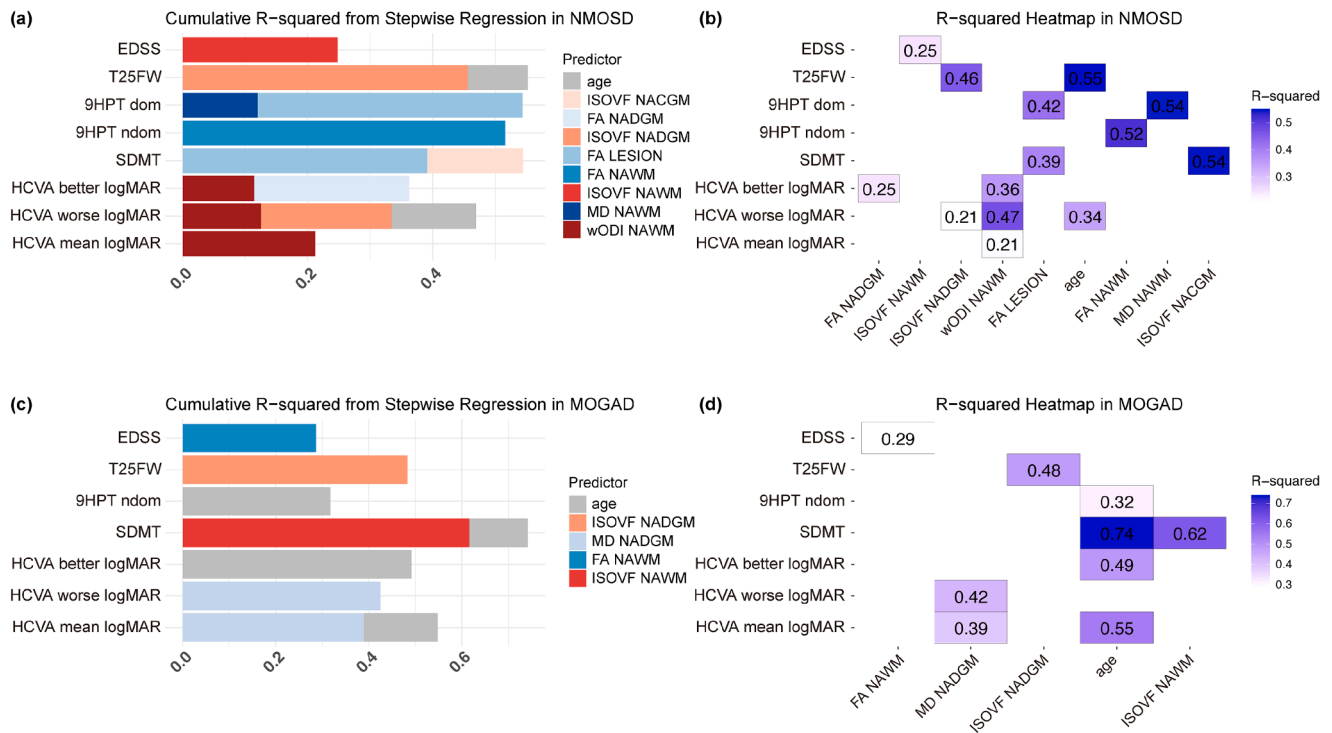
Fig. 4. Association of DTI and NODDI parameters with clinical disability in NMOSD and MOGAD.
(a) Bar plot of cumulative R-squared of predictors in each clinical parameter of NMOSD; (b) R-squared heatmap of each predictor in NMOSD; (c) Bar plot of cumulative R-squared of predictors in each clinical parameter in MOGAD; (d) R-squared heatmap of each predictor in MOGAD. In the R-squared heatmap, the darker the color, the higher the R-squared was. EDSS: Expanded Disability Status Scale; T25FW: Timed 25 Foot Walk; 9HPTdom, dominant hand of nine-hole peg test; 9HPTndom, nondominant hand of nine-hole peg test; SDMT: Symbol Digit Modalities Test; HCVA, High Contrast Visual Acuity; logMAR, logarithm of the Minimum Angle of Resolution; NMOSD: Neuromyelitis Optica Spectrum disorder; MOGAD: myelin oligodendrocyte glycoprotein antibody-associated disease; ISOVF: isotropic volume fraction; FA: fractional anisotropy; MD: mean diffusivity; wODI: tissue-weighted mean of orientation dispersion index; NACGM: normal appearing cortical gray matter; NADGM: normal appearing deep gray matter; NAWM: normal appearing white matter.

4. Discussion

This cross-sectional study investigated DTI- and NODDI-derived parameters in patients with MOGAD and NMOSD compared to controls, focusing on normal-appearing brain tissue and focal white matter lesions. We found (1) notable diffusion MRI alterations in lesions and cortical gray matter, but not in white matter during ROI-based analyses in both diseases. In contrast, TBSS revealed significantly higher AD, ODI, and ISOVF in WM tracts of NMOSD patients compared to controls, but not in MOGAD; (2) clinical outcomes in NMOSD patients were associated with both focal and diffuse microstructural alterations on diffusion MRI, whereas this association was less pronounced in MOGAD.

4.1. Multimodal diffusion MRI alterations

4.1.1. White matter lesions

In NMOSD, lesions showed increased MD, AD, and RD compared to controls, with similar trends observed in MOGAD patients. These results align with a prior study reporting increased MD and RD in NMOSD (Messina et al., 2022). Notably, our NODDI study revealed lower wNDI and higher ISOVF in lesions, reflecting the destructive nature of inflammatory plaques (Lucchinetti et al., 2014). This suggests that NODDI can detect disease-specific pathology in NMOSD or MOGAD, distinct from vascular-related lesions (Pantoni, 2010), as our controls had nonspecific cerebral small vascular-related lesions. Given that the median time since the last attack in our cohort exceeds six months (Table 1), the increase in water content is likely secondary to structural tissue damage. However ongoing inflammatory activity months or years after a clinical attack has also been reported with pathological data (Pisa et al., 2022; Takai et al., 2021).

4.1.2. Normal-appearing white matter

Prior research using DTI reported no white matter tract differences between NMOSD and MOGAD (Schmidt et al., 2020). Similarly, our ROI analysis of DTI and NODDI, found no significant white matter differences between both patient groups and compared to controls. This is partly consistent with a NODDI study of a larger sample size reporting no difference in whole-brain NAWM-ODI and NAWM-ISOVF between MOGAD and controls (Sun et al., 2023), yet they reported lower NAWM-NDI in AQP4+ NMOSD compared to HC.

Our TBSS findings showed increased AD in NMOSD relative to controls, particularly in the body of the corpus callosum, indicating altered white matter integrity. This contrasts with other studies showing no regional abnormality in AD compared with controls (Kim et al., 2017a), or increased AD across various WM fiber tracts (Yan et al., 2022). While no significant finding on NDI appeared, ODI and ISOVF alterations were concentrated in the corpus callosum and corona radiata in NMOSD, supporting previous reports of corpus callosum involvement (Kato et al., 2022) with higher ISOVF compared to controls. Although NAWM alterations may be interpreted in terms of inflammation or edema (Pisa et al., 2022), diffuse astrocyte pathology independent of demyelination or active inflammation has also been proposed (Misu et al., 2013). In contrast, MOGAD patients showed no significant differences compared to NMOSD or controls across white matter tracts. Notably, pediatric MOGAD patients tend to present acute disseminated encephalomyelitis (ADEM)-like features, while adult MOGAD are predominantly characterized by optic neuritis or myelitis (Reindl and Waters, 2019). This indicates that white matter may be less affected in adult MOGAD than in pediatric ADEM-like MOGAD. Moreover, our NMOSD patients had higher lesion loads than MOGAD patients, supporting more prominent white matter abnormalities in NMOSD.

4.1.3. Normal-appearing gray matter

In our study, cortical gray matter wNDI was lower in MOGAD compared to NMOSD, likely reflecting residual damage from previous cortical/subcortical gray matter lesions. In contrast, cerebral gray matter lesions are usually absent in NMOSD (Sinnecker et al., 2012), where brain lesions are mainly present in areas with high AQP4 expression, such as peri-ependymal areas, hypothalamus and area postrema (Dutra et al., 2018; Kim et al., 2015). In our study, 6 of 21 (29 %) MOGAD patients had cortical/juxtacortical lesions compared to only 1 NMOSD patient (Table 1), which aligns with results in other NMOSD cohorts (Duan et al., 2021; Messina et al., 2022).

Our findings of higher wODI but lower ISOVF in the cortical gray matter of NMOSD patients compared to controls suggest an abundance of reactive astrocytes with swollen cell bodies, as seen pathologically by Saji et al. (Saji et al., 2013b). However, hypertrophied astrocytes may contribute to increased intracellular volume, and restricted diffusion, like neurites, potentially overestimating NDI. Instead of a reduced NDI in MOGAD, the elevated NDI observed in NMOSD cortical regions may reflect both actual neurite density and contributions from hypertrophic astrocytes, warranting cautious interpretation.

4.2. Clinical associations

We found diffusion MRI biomarkers to be well associated with clinical disability in the NMOSD group, but to a lesser extent in the MOGAD group.

4.2.1. White matter

Higher EDSS was associated with higher white matter ISOVF in NMOSD and lower white matter FA in MOGAD, suggesting that diffusion MRI reflects chronic neuroinflammation and tissue damage. In NMOSD, worsening HCVA correlated with increased white matter wODI, suggesting that reduced visual acuity may relate to the loss of fiber coherence in visual tracts (e.g., optic radiation). Additionally, worse performance on the SDMT was associated with lower FA lesion in NMOSD, and higher ISOVF white matter in MOGAD, even after correcting for white matter volume, suggesting demyelination disrupts axonal conduction (Strober et al., 2019).

4.2.2. Gray matter

In NMOSD, worse SDMT performance was associated with higher ISOVF in cortical gray matter, supporting prior findings linking cognitive impairment to gray matter abnormalities (Kim et al., 2017b). Here, cognitive impairment was considered an attack-independent symptom. Diffuse cortical neuronal loss in NMOSD might result from the high AQP4 expression-induced gray matter damage (Saji et al., 2013a). Our findings support this hypothesis, showing that worsening SDMT correlates with ISOVF in cortical gray matter.

T25FW speed was strongly associated with ISOVF in deep gray matter for both NMOSD and MOGAD groups, supporting volumetric studies in NMOSD highlighting the role of thalamic and caudate atrophy in physical and cognitive disability (Hyun et al., 2017; Kim et al., 2017b).

In MOGAD, worsening HCVA was associated with increased MD deep gray matter, involving the lateral geniculate nucleus or the optic radiation connection to the primary visual cortex (Oertel et al., 2017).

4.3. Strengths and limitations

We utilized multi-dimensional approaches (tissue-weighted means of NODDI metrics and voxel-wise TBSS) to probe diffuse microstructural alterations in NABT and WML in NMOSD and MOGAD. Limitations included a clinically stable cohort of NMOSD and MOGAD patients rather than in the acute stage at the time of the visit, which may limit the consistency of our findings with previous ones, as well as a cross-sectional monocentric design with an exclusively Caucasian cohort limiting generalizability. Ethnic differences in NMOSD presentation are not limited to prevalence alone and include lower incidence of brain/brainstem involvement in Caucasians compared to Asians (Kim et al., 2018). Lastly, while the correlation between DTI/NODDI metrics and clinical outcomes highlights the potential clinical relevance of these findings, it remains challenging to interpret how each clinical score relates to MRI parameters in addition to multicollinearity among diffusion metrics. This warrants careful selection and interpretation of clinical measures with specific MRI metrics, as each clinical measure involves multiple neuronal pathways and distinct functional anatomical structures.

5. Conclusion

Patients with NMOSD and MOGAD exhibit similar cerebral microstructural differences compared to controls as indicated by NODDI metrics. However, NMOSD patients show more extensive residual white matter microstructural changes, while MOGAD patients presented less underlying tissue damage, providing a tentative explanation for on average better clinical outcomes in MOGAD. NODDI, as a novel diffusion model, effectively identifies neurite damage and neuroinflammation and may be more sensitive and specific to alterations in NACGM than DTI. The association of NODDI metrics with clinical disability highlights their potential as valuable surrogate neuroimaging biomarkers in clinical research.

CRediT authorship contribution statement

Qianlan Chen: Writing – original draft, Methodology, Formal analysis, Data curation. **Henri Trang:** Writing – review & editing, Formal analysis. **Patrick Schindler:** Data curation. **Frederike Cosima Oertel:** Writing – review & editing, Methodology, Data curation. **Tim Hartung:** Data curation. **Darius Mewes:** Data curation. **Claudia Chien:** Writing – review & editing, Data curation. **Stefan Hetzer:** Writing – review & editing. **Lina Anderhalten:** Writing – review & editing. **Michael Sy:** Writing – review & editing. **Carsten Finke:** Writing – review & editing, Data curation. **Tanja Schmitz-Hübsch:** Writing – review & editing, Methodology, Data curation. **Alexander U. Brandt:** Writing – review & editing, Supervision, Conceptualization. **Friedemann Paul:** Writing – review & editing, Supervision, Conceptualization.

Declaration of competing interest

Qianlan Chen has received a scholarship from China Scholarship Council (CSC). Henri Trang was supported by iNAMES - MDC - Weizmann - Helmholtz International Research School for Imaging and Data Science from NAno to MESo. Patrick Schindler has received travel support by UCB, and received speaker's honoraria by Roche and Alexion and he served on an advisory board by Alexion. Frederike C. Oertel has received research funding from the American Academy of Neurology (AAN) and the National MS Society (NMSS) as well as the German Association of Neurology (DGN). She currently receives research funding from the Hertie foundation for excellence in clinical neurosciences, the German Research Association (DFG) TWAS program, and Novartis UG. She received speaking honoraria from UCB. Tim Hartung has nothing to disclose. Darius Mewes has received a research scholarship from the Berlin Institute of Health at Charité, Berlin, Germany. Claudia Chien has received research support from Novartis and Alexion, AstraZeneca Rare Disease, is a Standing Committee on Science Member for the Canadian

References

Alexander, A.L., Lee, J.E., Lazar, M., et al., 2007. Diffusion tensor imaging of the brain. Neurotherapeutics. 4 (3), 316–329.

Andica, C., Hagiwara, A., Yokoyama, K., et al., 2022. Multimodal magnetic resonance imaging quantification of gray matter alterations in relapsing-remitting multiple sclerosis and neuromyelitis optica spectrum disorder. J. Neurosci. Res.

Bagdasarian, F.A., Yuan, X., Athey, J., et al., 2021. NODDI highlights recovery mechanisms in white and gray matter in ischemic stroke following human stem cell treatment. Magn. Reson. Med. 86 (6), 3211–3223.

Banwell, B., Bennett, J.L., Marignier, R., et al., 2023. Diagnosis of myelin oligodendrocyte glycoprotein antibody-associated disease: international MOGAD Panel proposed criteria. Lancet Neurol. 22 (3), 268–282.

Daducci, A., Canales-Rodriguez, E.J., Zhang, H., et al., 2015. Accelerated microstructure imaging via Convex optimization (AMICO) from diffusion MRI data. Neuroimage 105, 32–44.

Duan, Y., Zhuo, Z., Li, H., et al., 2021. Brain structural alterations in MOG antibody diseases: a comparative study with AQP4 seropositive NMOSD and MS. J. Neurol. Neurosurg. Psychiatry 92 (7), 709–716.

Dutra, B.G., da Rocha, A.J., Nunes, R.H., et al., 2018. Neuromyelitis optica spectrum disorders: spectrum of MR imaging findings and their differential diagnosis. Radiographics. 38 (1), 169–193.

Grobelny, A., Behrens, J., Mertens, S., et al., 2017. Maximum walking speed in multiple sclerosis assessed with visual perceptive computing. PLoS. One 12 (12), e0189281.

Haddad, S.M.H., Scott, C.J.M., Ozzoude, M., et al., 2022. Comparison of diffusion tensor imaging metrics in normal-appearing white matter to cerebrovascular lesions and correlation with cerebrovascular disease risk factors and severity. Int. J. Biomed. ImAging 2022, 5860364.

Heine, J., Schwichtenberg, K., Hartung, T.J., et al., 2023. Structural brain changes in patients with post-COVID fatigue: a prospective observational study. EClinicalMedicine 58, 101874.

Henschel, L., Conjeti, S., Estrada, S., et al., 2020. FastSurfer - A fast and accurate deep learning based neuroimaging pipeline. Neuroimage 219, 117012.

Hyun, J.W., Park, G., Kwak, K., et al., 2017. Deep gray matter atrophy in neuromyelitis optica spectrum disorder and multiple sclerosis. Eur. J. Neurol. 24 (2), 437–445.

Jarius, S., Paul, F., Aktas, O., et al., 2018. MOG encephalomyelitis: international recommendations on diagnosis and antibody testing. J. Neuroinflammation. 15 (1), 134.

Jarius, S., Paul, F., Weinshenker, B.G., et al., 2020. Neuromyelitis optica. Nat. Rev. Dis. Primers. 6 (1), 85.

Kato, A., Hagiwara, A., Yokoyama, K., et al., 2022. Microstructural white matter abnormalities in multiple sclerosis and neuromyelitis optica spectrum disorders: evaluation by advanced diffusion imaging. J. Neurol. Sci. 436, 120205.

Kim, H.J., Paul, F., Lana-Peixoto, M.A., et al., 2015. MRI characteristics of neuromyelitis optica spectrum disorder: an international update. Neurology. 84 (11), 1165–1173.

Kim, S.H., Kwak, K., Hyun, J.W., et al., 2017a. Diffusion tensor imaging of normal-appearing white matter in patients with neuromyelitis optica spectrum disorder and multiple sclerosis. Eur. J. Neurol. 24 (7), 966–973.

Kim, S.H., Mealy, M.A., Levy, M., et al., 2018. Racial differences in neuromyelitis optica spectrum disorder. Neurology. 91 (22), e2089–e2099.

Kim, S.H., Park, E.Y., Park, B., et al., 2017b. Multimodal magnetic resonance imaging in relation to cognitive impairment in neuromyelitis optica spectrum disorder. Sci. Rep. 7 (1), 9180.

Lakens, D., 2013. Calculating and reporting effect sizes to facilitate cumulative science: a practical primer for *t*-tests and ANOVAs. Front. Psychol. 4.

Lamers, I., Cattaneo, D., Chen, C.C., et al., 2015. Associations of upper limb disability measures on different levels of the International Classification of functioning, disability and health in people with Multiple sclerosis. Phys. Ther. 95 (6), 65–75.

Lucchinetti, C.F., Guo, Y., Popescu, B.F., et al., 2014. The pathology of an autoimmune astrocytopathy: lessons learned from neuromyelitis optica. Brain Pathol. 24 (1), 83–97.

Messina, S., Mariano, R., Roca-Fernandez, A., et al., 2022. Contrasting the brain imaging features of MOG-antibody disease, with AQP4-antibody NMOSD and multiple sclerosis. Mult. Scler. 28 (2), 217–227.

Michael P, H., Leah H, S., Beau M, A., et al., 2018. Extending the Human Connectome Project across ages: imaging protocols for the Lifespan Development and Aging projects. Neuroimage 183, 972–984.

Misu, T., Hoftberger, R., Fujihara, K., et al., 2013. Presence of six different lesion types suggests diverse mechanisms of tissue injury in neuromyelitis optica. Acta Neuropathol. 125 (6), 815–827.

Mitchell, T., Wilkes, B.J., Archer, D.B., et al., 2022. Advanced diffusion imaging to track progression in Parkinson's disease, multiple system atrophy, and progressive supranuclear palsy. Neuroimage Clin. 34, 103022.

Mori, S., Oishi, K., Jiang, H., et al., 2008. Stereotaxic white matter atlas based on diffusion tensor imaging in an ICBM template. Neuroimage 40 (2), 570–582.

Oertel, F.C., Kuchling, J., Zimmermann, H., et al., 2017. Microstructural visual system changes in AQP4-antibody-seropositive NMOSD. Neurol. Neuroimmunol. Neuroinflamm. 4 (3), e334.

Pantoni, L., 2010. Cerebral small vessel disease: from pathogenesis and clinical characteristics to therapeutic challenges. Lancet Neurol. 9 (7), 689–701.

Papadopoulos, M.C., Verkman, A.S., 2012. Aquaporin 4 and neuromyelitis optica. Lancet Neurol. 11 (6), 535–544.

Parker, C.S., Veale, T., Bocchetta, M., et al., 2021. Not all voxels are created equal: reducing estimation bias in regional NODDI metrics using tissue-weighted means. Neuroimage 245, 118749.

Pisa, M., Pansieri, J., Yee, S., et al., 2022. Anterior optic pathway pathology in CNS demyelinating diseases. Brain 145 (12), 4308–4319.

Rahmanzadeh, R., Lu, P.J., Barakovic, M., et al., 2021. Myelin and axon pathology in multiple sclerosis assessed by myelin water and multi-shell diffusion imaging. Brain 144 (6), 1684–1696.

Reindl, M., Waters, P., 2019. Myelin oligodendrocyte glycoprotein antibodies in neurological disease. Nat. Rev. Neurol. 15 (2), 89–102.

Saji, E., Arakawa, M., Yanagawa, K., et al., 2013a. Cognitive impairment and cortical degeneration in neuromyelitis optica. Ann. Neurol. 73 (1), 65–76.

Saji, E., Arakawa, M., Yanagawa, K., et al., 2013b. Cognitive impairment and cortical degeneration in neuromyelitis optica. Ann. Neurol. 73 (1), 65–76.

Schmidt, F.A., Chien, C., Kuchling, J., et al., 2020. Differences in advanced Magnetic resonance imaging in MOG-IgG and AQP4-IgG seropositive neuromyelitis optica spectrum disorders: a comparative study. Front. Neurol. 11, 499910.

Sinnecker, T., Dörr, J., Pfueller, C.F., et al., 2012. Distinct lesion morphology at 7-T MRI differentiates neuromyelitis optica from multiple sclerosis. Neurology. 79 (7), 708–714.

Smith, S., Jenkinson, M., Johansen-Berg, H., et al., 2006. Tract-based spatial statistics: voxelwise analysis of multi-subject diffusion data. Neuroimage 31 (4), 1487–1505.

Sperber, P.S., Brandt, A.U., Zimmermann, H.G., et al., 2022. Berlin Registry of Neuroimmunological entities (BERLimmun): protocol of a prospective observational study. BMC. Neurol. 22 (1).

Strober, L., DeLuca, J., Benedict, R.H., et al., 2019. Symbol digit Modalities Test: a valid clinical trial endpoint for measuring cognition in multiple sclerosis. Mult. Scler. 25 (13), 1781–1790.

Sun, J., Xu, S., Tian, D., et al., 2023. Periventricular gradients in NAWM abnormalities differ in MS, NMOSD and MOGAD. Mult. Scler. Relat. Disord. 75, 104732.

Takai, Y., Misu, T., Suzuki, H., et al., 2021. Staging of astrocytopathy and complement activation in neuromyelitis optica spectrum disorders. Brain 144 (8), 2401–2415.

Tournier, J.D., Smith, R., Raffelt, D., et al., 2019. MRtrix3: a fast, flexible and open software framework for medical image processing and visualisation. Neuroimage 202, 116137.

Wheeler-Kingshott, C.A.M., Cercignani, M., 2009. About "axial" and "radial" diffusivities. Magn. Reson. Med. 61 (5), 1255–1260.

Wingerchuk DM, B.B., Bennett, J.L, Cabre, P., Carroll, W., Chitnis, T., de Seze, J., Fujihara, K., Greenberg, B., Jacob, A., Jarius, S., Lana-Peixoto, M., Levy, M.,

Simon, J.H., Tenembaum, S., Traboulsee, A.L., Waters, P., Wellik, K.E., Weinshenker, B.G., 2015. International Panel for NMO Diagnosis. International consensus diagnostic criteria for neuromyelitis optica spectrum disorders. Neurology. 85 (2), 177–189.

Yan, Z., Wang, X., Zhu, Q., et al., 2022. Alterations in white matter Fiber tracts characterized by automated Fiber-tract quantification and their correlations with cognitive impairment in Neuromyelitis Optica spectrum disorder patients. Front. Neurosci. 16, 904309.

Yushkevich, P., Gao, Yang, Gerig, G., 2016. ITK-SNAP: an interactive tool for semi-automatic segmentation of multi-modality biomedical images. In: Annual International Conference of the IEEE Engineering in Medicine and Biology Society. IEEE Engineering in Medicine and Biology Society. Annual International Conference 2016, pp. 3342–3345.

Zhang, H., Schneider, T., Wheeler-Kingshott, C.A., et al., 2012. NODDI: practical in vivo neurite orientation dispersion and density imaging of the human brain. Neuroimage 61 (4), 1000–1016.